33RD CONGRESS
OF THE INTERNATIONAL COUNCIL
OF THE AERONAUTICAL SCIENCES
STOCKHOLM, SWEDEN, 4-9 SEPTEMBER, 2022

ICAS 2022 SWEDEN

Fatigue characterization of adhesive joints in aeroplanes – the development of a negative load ratio (R<0) testing method

Olli Orell[1], Jarno Jokinen[1], Mikko Kanerva[1]

[1]Faculty of Engineering and Natural Sciences, Tampere University, Finland

Abstract

Adhesive joints are an efficient method to transfer high loads between structural components. High-performing adhesive joints require careful design and precise knowledge of the adhesive product used. Especially in aeroplanes, load spectra range from negative to positive load (factor) levels. It is well known that the trajectory of crack growth in adhesive joints is highly sensitive to local stress state and fracture toughness. However, up to date, there are no methods to accurately study fatigue of adhesive joints under varying load (positive-to-negative loading, i.e., load ratio R changing its sign). In this study, a testing system is developed to perform negative R fatigue testing of adhesive joints and mode II crack propagation.

Keywords: joints, fatigue, crack propagation, adhesive

1. Introduction

Adhesive bonding is a widely used joining technique in aeroplane structures. Aeroplane structures need to sustain fatigue loading during the overall lifespan, which can be several decades. This requirement is also valid when defects exist in the joint. For understanding the damage in bonded joints and the related damage tolerance, experimental testing is needed. Especially, the fracture mode II has recently been under intensive research in the scientific literature.

The fracture mode II testing has not been established while steps towards standardization has been taken. The testing and analysis of the fracture mode II in general has been performed by using various specimens and test setups [1]. These include End Loaded Split [2], Tapered End Notched Flexure [3] and End Notched Flexure (ENF) [4]. The published works have indicated differences between specimens, e. g., related to friction [5]. Probably, the most common test specimen configuration for fatigue testing of adhesives is ENF. The main challenge in the mode II testing has been the definition and observation of crack length. The numerical post-processing methods based on the specimen compliance have typically been applied [6]. However, new methods for post-processing and monitoring have been developed. Digital Image Correlation (DIC) has been studied for observing fatigue crack propagation [7].

The fatigue loading cannot be ignored when considering the damage tolerance of adhesive bonded joints in aeroplanes. There is a demand for experimental data for estimating the structural integrity. Similar features, as indicated earlier, occurs in static and fatigue loadings under mode II as has been studied in a number of works [8], [9]. However, the published works have mainly been focused on a positive load ratio (R). In real-life joints, the loading can have a negative load ratio and the testing with positive R might provide a non-conservative estimate (Fig. 1). This is a significant gap of knowledge in the current literature. The negative load ratio (R<0) does not happen without challenges of testing. The main challenge is to create boundary conditions, which are not restricting the target deformation in the joint. The rigid-body motion of the specimen should still be restricted when the load removal occur (when R changes its sign).

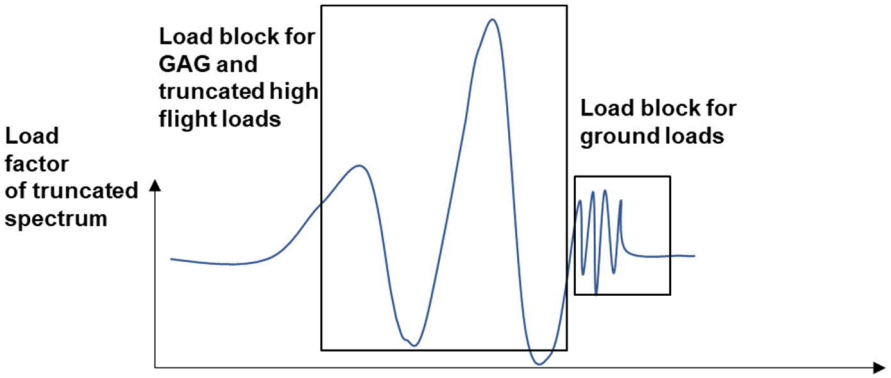

Figure 1 – Typical fatigue spectra of testing and truncation for fatigue studies of aeroplanes. Modified based on data in [10], [11].

In this work, the fracture mode II for adhesive and related test setup for a negative load ratio was studied. The developed test setup was designed based on the ENF specimen. The challenge in the negative load ratio is to support the specimen correctly but to let the joint (adhesive along the glue line) deform properly. Typically, the removal of the loading when the sign (of load) changes upon cyclic loading allows movement of the specimen – this should be avoided or considered properly. However, the fixing of specimen should not restrict specimen deformations so that adhesive behaviour is modified. Our target was to study the developed test arrangement and its applicability in $R<0$ testing. The test jig and the specimen deformations were studied using DIC. The test jig deformations were also analysed using finite element method. In addition, preliminary fatigue tests were successfully performed with the new setup. These results were compared to the results by a traditional three-point flexure fixture. The negative load ratio (R) related test characterized the influence of the fixture on the crack propagation. The crack propagation was shown to be significant when compared to the tests of positive load ratio and same load level.

2. Materials and methods

2.1 Test setup

For correctly designed joints, the adhesive layer will carry shearing loads and experience mode II fracture in the event of damage. The ENF specimen benefit its simplicity in terms of the load introduction when only the three-point bending fixture is needed. The traditional three-point ENF setup does not allow negative load ratios where the load direction is changing (for fatigue testing). In this work, additional supports were added on both sides of the specimen. The concept is basically creating a mirror structure making the loading and the jig itself symmetric. The designed test jig is shown in Fig. 2. The challenge of the test jig is the specimen longitudinal movement. This should be minimized which is the case also with restrictions on supports preventing free bending. The final test setup had 50 µm gap between the specimen and unloaded supports at the beginning. This influence on horizontal movement was confirmed using DIC.

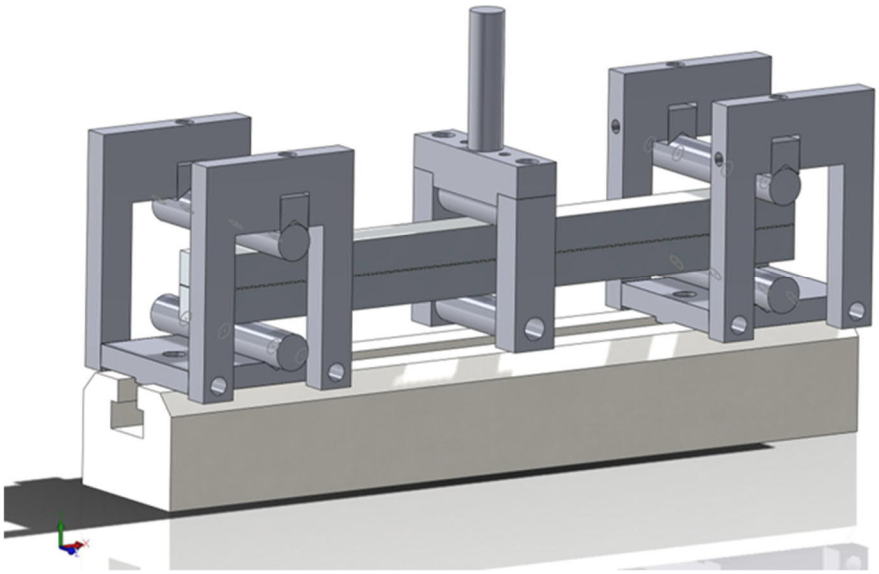

Figure 2 – The test setup and jig design for *R*<0 testing of ENF adhesively bonded specimen.

2.2 Specimen and testing

The ENF specimen used here, for test jig validation, included aluminium adherends and two layers of FM 300-2 (Solvay) adhesive film between the adherends. The ENF specimen behaviour was analysed in the previous work by Jokinen et al. [12]. For the precrack preparation, a release film was placed between the two layers of adhesive film. The exact specimen dimensions are shown in Fig. 3. The specimen width was 15 mm, the thickness of adhesive (total glue line) was 0.6 mm, and the precrack length was 108 mm. Additionally, DIC was used to collect displacement and strain field data (the field on the side surface of the entire test arrangement). For this, a paint pattern was applied over the entire side surface to form proper intensity changes (gray-scale vision) during camera recording. The camera data was analysed using the DaVis 10.0.5 software (LaVision, Germany) software.

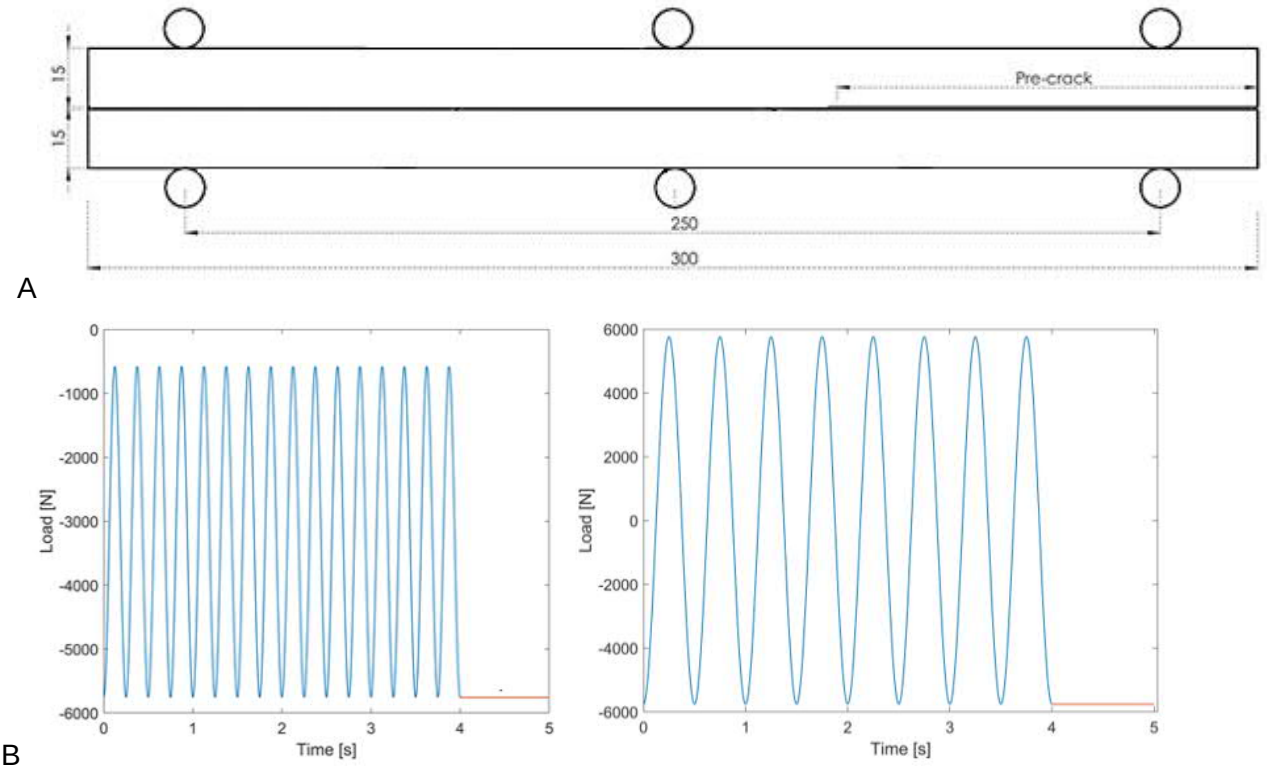

Figure 3 – A: The ENF test specimen for studying *R*<0 fatigue. B: Repeating fatigue cycle patterns for *R*=0.1 and *R*=-1 test cases.

In the test program, the maximum (peak) load was 5.8 kN and covered 60 % of the static strength (quasi-static maximum force 9.6 kN). Three different loading scenarios were applied using three separate specimens to entirely distinguish loading-specific changes in behaviour. The first scenario was cyclic loading for both upwards (i.e., against gravity) and downwards direction (R=0.1) by using the new test setup. The target of the scenario was to collect comparison data for load direction related effects. Another scenario was testing under R=-1 cyclic (fatigue) loading. These scenarios and the gained data were compared to the reference testing, which was applied in the traditional three-point bending test setup *without* the ability to change the load direction. In addition, the 50 % load level results for R=-1 and R=0.1 are presented. A universal servo-hydraulic testing machine (Instron) was used for loading.

2.3 Finite element model

The three-dimensional finite element (FE) model was made using Abaqus/Standard 2021 (Simulia). The target of the model was to analyse the test jig deformations. The FE model consisted of the test jig and the ENF specimen as shown in Fig. 4. The ENF specimen included aluminium adherends and adhesive. The test jig and specimen adherends were modelled using linear elastic properties. Aluminium Young's modulus was 71 GPa and Poisson's ratio 0.3. The adhesive was modelled using elastic and, alternatively, elastic-plastic properties. The adhesive's Young's modulus was 2.45 GPa and Poisson's ratio 0.38. The elastic-plastic behaviour was estimated as linear elastic ideally plastic with the yield strength of 53 MPa [13]. The test jig was simplified for the FE analysis: The test jig was merged into one part, excluding bolts joining jig parts. This might have affected slightly the load division between the outer supports. The outer lower supports were also not modelled when the (vertical) upward loading was studied.

The contact between the ENF specimen and supports were defined using frictionless surface to surface contact. Adhesive and adherends were joined using the 'tie constraint'. The pre-crack was modelled in the middle of the adhesive using the Virtual Crack Closure Technique (VCCT). Two crack lengths were considered in analysis presenting the initial pre-existing crack (108 mm from the specimen edge) and when the crack has propagated close to the centre loading point (145 mm from the specimen edge). The test jig's boundary conditions were attached to the whole lower surface restricting all displacements (Fig. 4). The upper end surface of the centre loading part was made rigid and the reference point was added. For the reference point, displacements and rotations were restricted excluding the vertical displacement. The vertical enforced displacement was placed into the reference point. The enforced displacement was used for improving the convergence of the model during solving the simulation. The value of the displacement was fitted for presenting 5.8 kN load. The ENF specimen's boundary conditions were attached along the width direction (a nodal line). The nodal line was located at the top of the specimen, in the longitudinal direction to the middle. The displacement in the longitudinal and width direction was restricted along this line. The FE model was meshed using linear solid tetrahedral and hexahedral elements (C3D4, C3D8R & C3D10). Tetrahedral elements are not optimal for stress analysis and typically hexahedral element shapes are preferred. This might be difficult when complex geometries are meshed, such as the test jig. The specimen had rectangular shape for which hexahedral were applicable. The typical element dimension was 5 mm, which provided 101,281 elements in total.

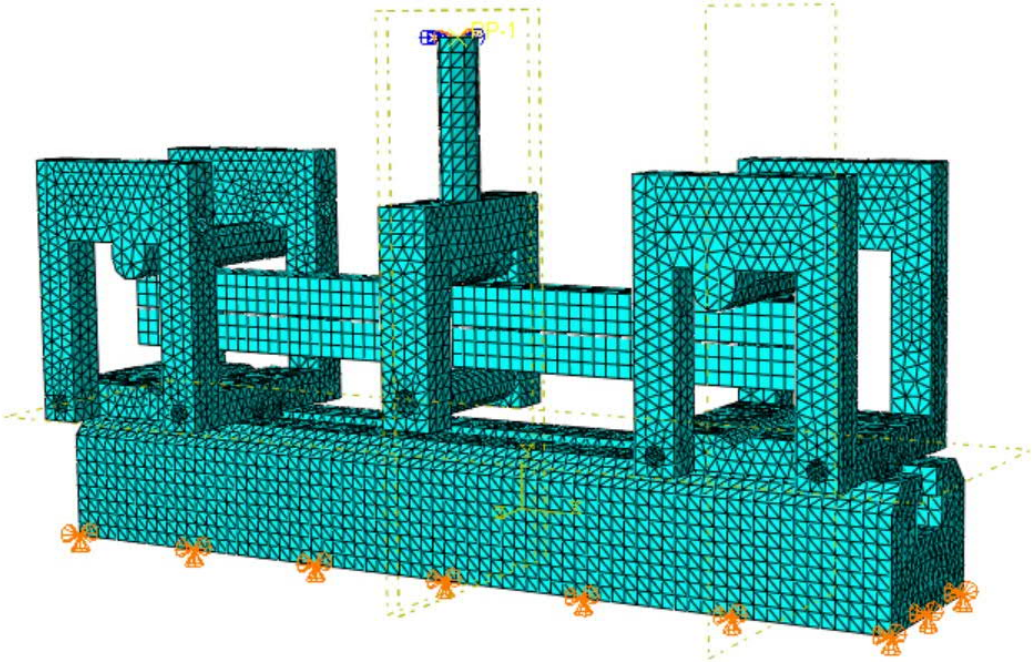

Figure 4 – The three-dimensional finite element model including the new test jig and an ENF specimen. The element mesh and boundary conditions are also visible.

3. Results

3.1 Deformation of the test jig

DIC was used for studying the deformations in the test setup under static loading. The specimen was mechanically tested before DIC data collection, and the crack had reached the longitudinal middle point. Then, the loading was performed in both directions (upwards and downwards movement of the machine crosshead). Figure 5 presents the vertical (coincide with upward movement of the crosshead) and horizontal deformations under both loading directions as provided using the DIC technique. The horizontal deformations of the test setup are around 0.1 mm. The system's vertical deformations are in the range of 1.0 mm. Based on these DIC measurements, the test setup does not have unexpected deformations during quasi-static loadings for negative and positive load directions.

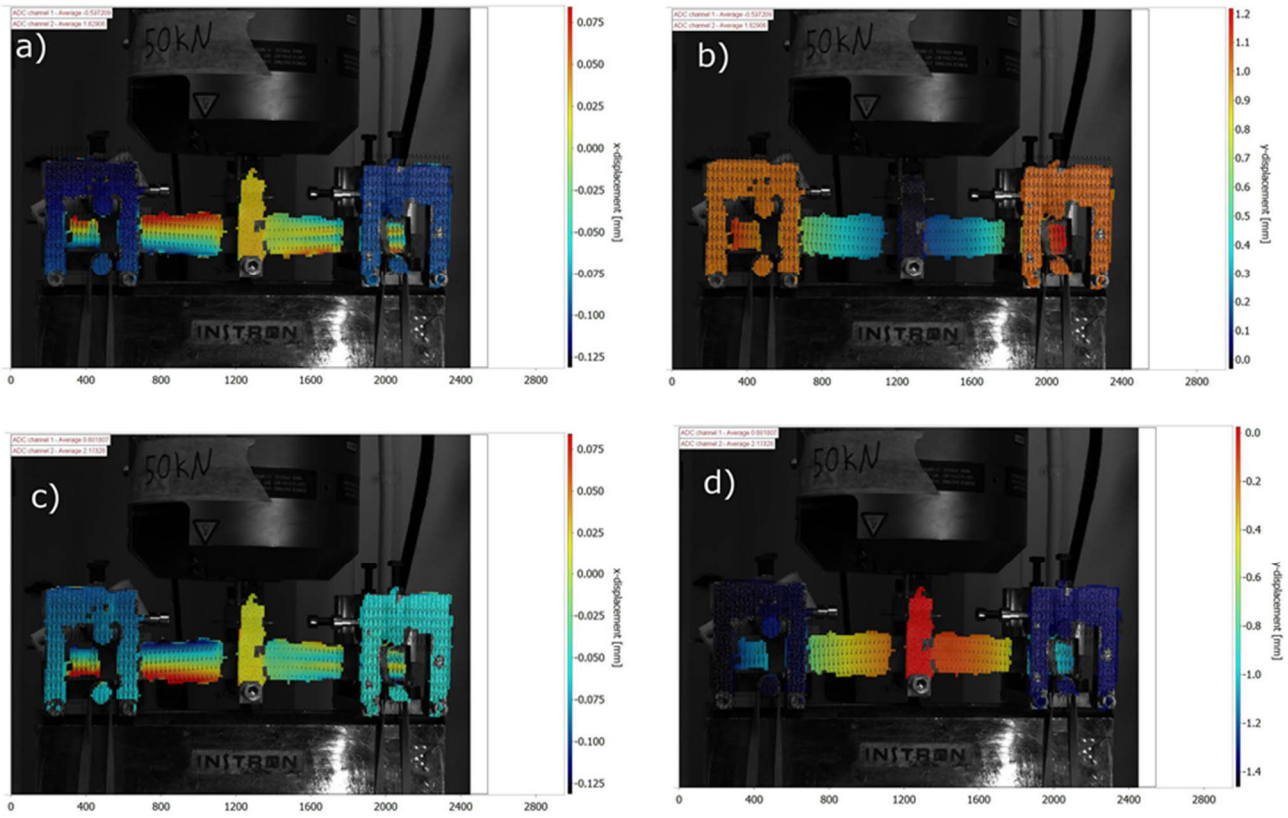

Figure 5 – The measured deformations of the test setup: a) horizontal displacement (at -6 kN), b) vertical displacement (at -6 kN), c) horizontal displacement (at +6 kN) and d) vertical displacement (at +6 kN). In the figure units are given in millimetres. Positive directions upwards and rightwards. The central loading pin is stationary, which means that the rest of the test setup is moving (connected to the test machine's hydraulic cylinder).

3.2 Horizontal movement of the specimen

The main challenge in the negative *R* testing is the load direction change, which requires momentary removal of the load (change of load sign). The specimen is not fixed in the horizontal direction and the movement in the specimen longitudinal direction might exist. During the preliminary testing, outer supports were not clamped in *R*<0 testing. The horizontal movement was studied using DIC in this work. Based on the DIC results, small horizontal movement was observed. Figure 6 presents horizontal displacement for the *R*=-1 test (50 % loading). Figure 6 indicates 0.8 mm of displacement in the horizontal direction when the crack has propagated close to the centre loading point. The horizontal movement was similarly studied in other specimens and no repeating trend of movement was observed. However, the initial movement was also observed in the positive load ratio tests.

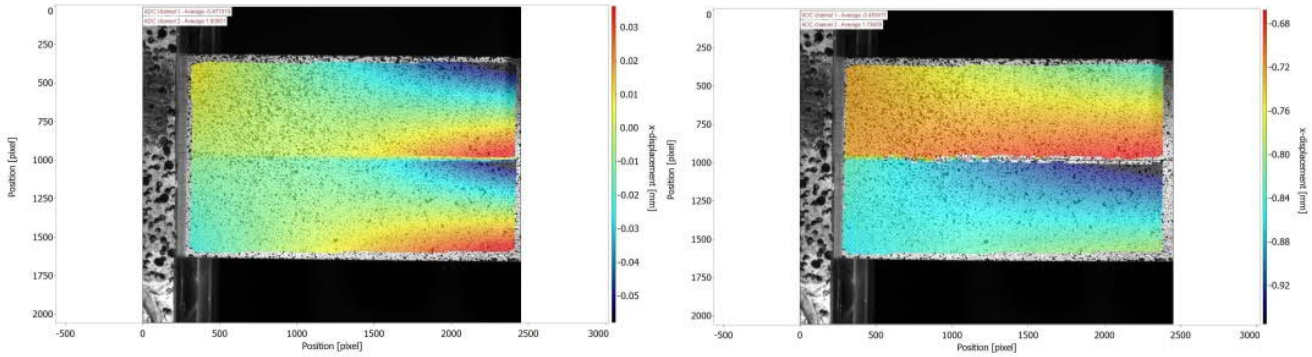

Figure 6 – The horizontal displacement of the specimen during the tests *R*=-1 (50 %): at the beginning (left) and at the end of the test (right).

3.3 FE results

The horizontal and vertical displacements of the elastic FE model are shown in Figs. 7 and 8, respectively. The FE analyses were performed for two cases with different crack lengths. The crack is located on the left side of the ENF specimen in Figs. 7 and 8. The horizontal displacements for the crack length of 108 mm and 145 mm are shown in Fig. 7. The horizontal displacement's maximum values are found in the ENF specimen while the test jig's horizontal deformation remains low. The ENF-related boundary conditions were placed for FE modelling at the longitudinal middle nodal line on the top of the specimen. The ENF specimen's horizontal displacement is higher when the crack length of 145 mm is studied. The maximum and minimum are found in the opposite location to the crack side and close to the bond line in the ENF specimen's ends.

The vertical displacements of the test jig are reported in Fig. 8. The vertical upwards displacement of the jig is less than 0.1 mm, which is insignificant deformation (less than 3 % of total ENF test amplitude). Total ENF amplitude is the displacement at boundary condition in the FE model. The FE analyses confirm that the designed test jig's deformation remain low and the test jig is enough stiff for actual standard testing. When the current middle support is also included in the analysis, the jig's deformation remains low (less than 5 % of total ENF test amplitude). It is important to note, that downwards loading results in clearly lower deformation in the jig due to the bulky support rail. The support rail transfers the loads from the two outer support pins to the test machine.

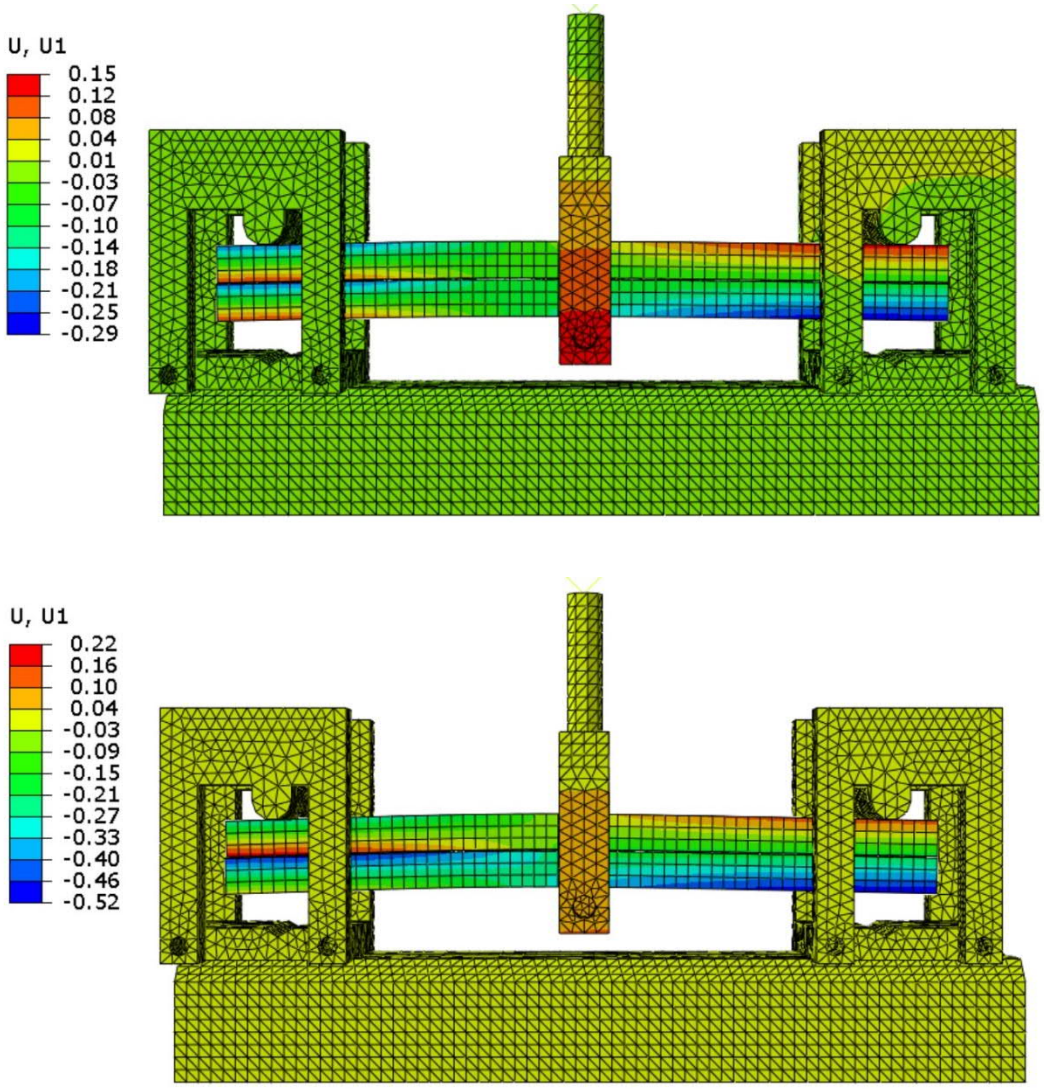

Figure 7 – The horizontal displacement (U1): the case of crack length 108 mm (top) and 145 mm (bottom) (units in mm).

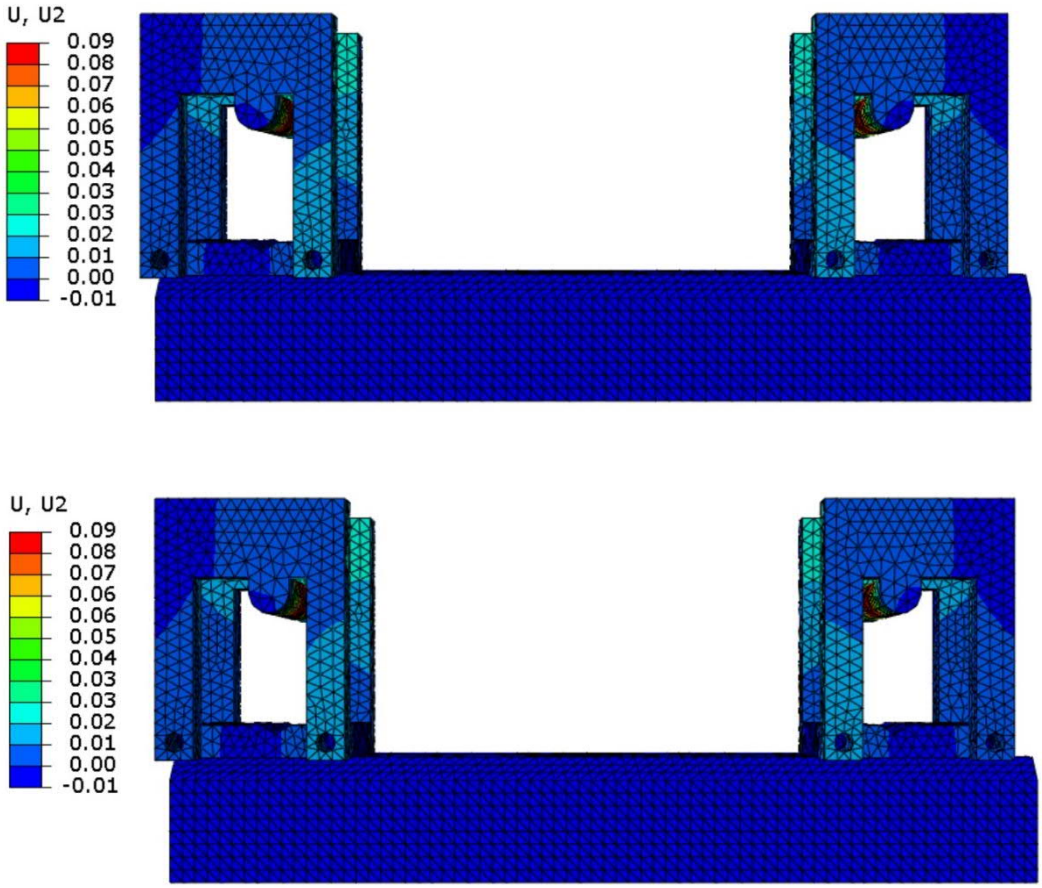

Figure 8 – The vertical displacement (U2) of the test jig: the case of crack length 108 mm (top) and 145 mm (bottom) from the edge (units in mm).

Elastic-plastic material model was also used for adhesive. The horizontal displacement for the crack length (108 mm) is shown in Fig. 9. The comparison between Figs. 7 and 9 indicates only small difference in the horizontal displacement. This is intuitive when specimen adherends are relatively thick and stiff when compared to the adhesive. FE analysis provides larger horizontal deformation than experiments (Fig. 5 c and d). However, the agreement related to the horizontal deformation of FE analysis and experiments are in the same scale (millimeter tenths). The experimental test setup is moving, which is shown as a vertical shift in the DIC. The specimen is removed from FE visualization for characterizing the test jig deformation.

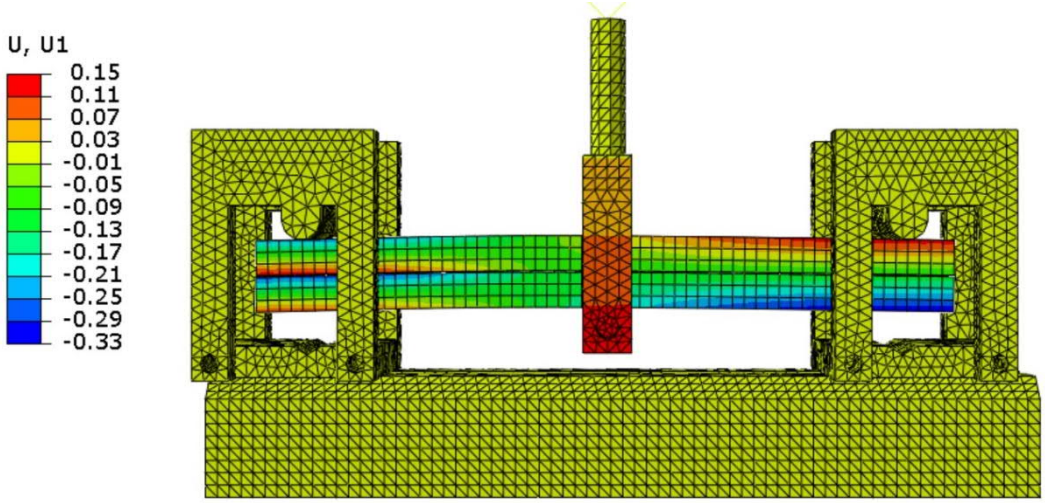

Figure 9 – The horizontal displacement (U1): the case of crack length 108 mm (units in mm). The elastic-plastic material model for adhesive is used.

3.4 Fatigue testing

Fatigue testing and related results are shown in Fig. 10. The results are shown using dynamic stiffness (dF/dS, S_d). Dynamic stiffness is defined as

$$S_d = dF/dS \quad (1)$$

where ΔF is the difference between maximum and minimum force and ΔS is the crosshead displacement for one load cycle. All the four studied load case scenarios, shown in Fig. 10, have been performed for the same absolute load level (60 %). Figure 10 presents that the dynamic stiffness of the new test setup is 10-15 % higher in the compression direction (here downwards movement) than in the other direction. The traditional three-point bending setup has its stiffness value between the two curves by the new system. The shape of the curve in the *R*=0.1 scenarios are similar to each other. The dynamic stiffness is decreasing first only slightly until the rate change becomes clearly faster. Based on these results, the new testing setup for the (upwards) tensile load seems to provide slightly faster crack propagation (than other *R*=0.1 test scenarios). The compression (downwards) has an opposite effect. The fatigue testing with a negative load ratio (*R*=-1) is distinct when compared to the positive load ratio (*R*=0.1) testing (either direction). The crack propagation (when *R*=-1) is significantly faster when the cycle count is less than 1,000 cycles. The dynamic stiffness vs cycles for the 50 % load level is shown in Fig. 11. The negative load ratio (*R*=-1) is shown to have significantly faster changes when compared to the positive load ratio (*R*=0.1).

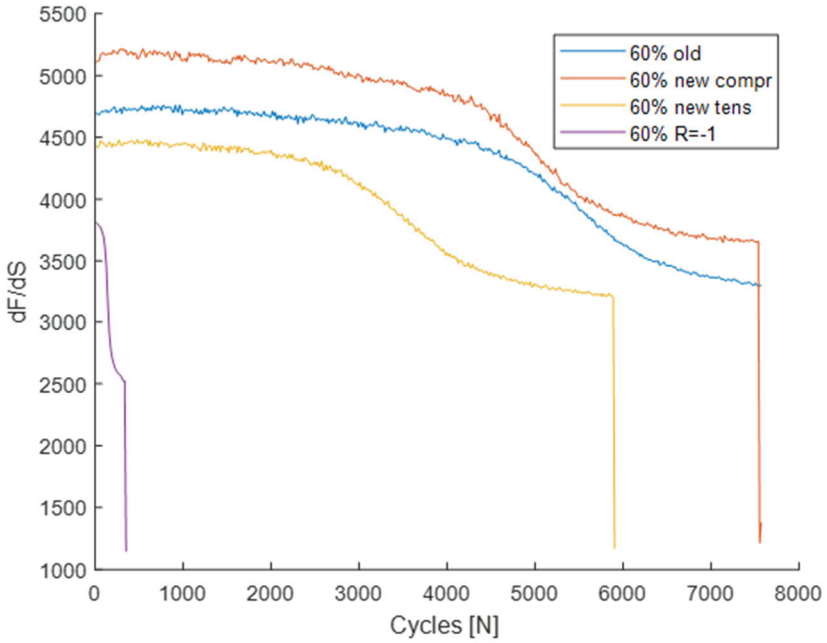

Figure 10 – Fatigue testing and study of dynamic stiffness versus number of cycles. The 60 % load level with the marking 'old' is for the traditional three-point bending setup. The 60 % 'new compr' and 'tens' are the markings for tests by using the new setup with the test machine working in downwards and upwards direction, respectively. The new setup and testing at the 60 % peak load level and at *R*=-1 is marked with '*R*=-1'.

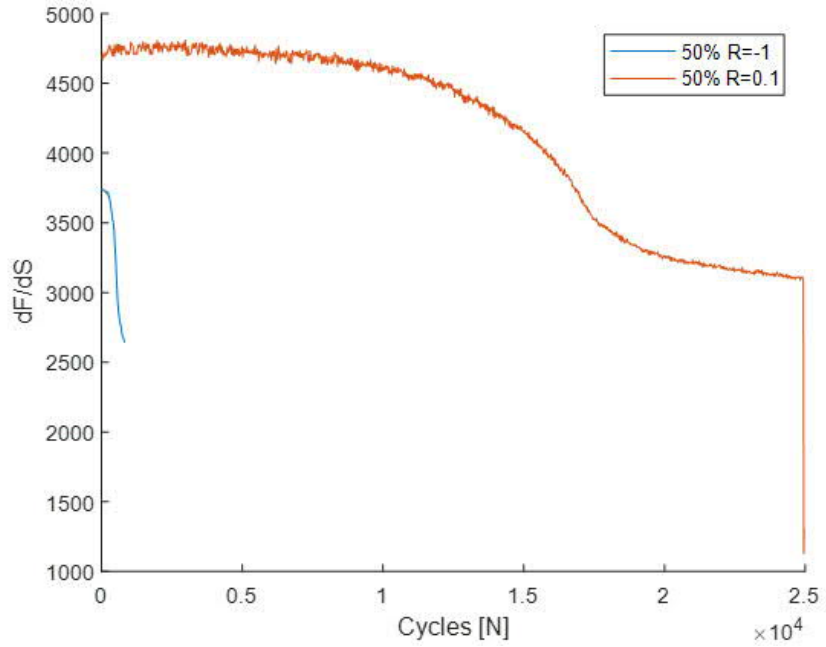

Figure 11 – Fatigue testing and study of the dynamic stiffness versus number of cycles when using the 50 % load level and different load ratio.

3.5 Fracture surface

The DIC-measured shear strain distribution at the last phase of test is shown in Fig. 12. The distribution shows that the crack propagation has basically been jumping between the upper and lower adhesive-adherend interfaces during testing. The same observation was made when analysing the post-test fracture surfaces (Fig. 13). The negative load ratio-related testing provided more rough surfaces when compared to the tests with a positive load ratio. The positive load ratio related testing also showed typically crack propagation which propagated close to one interface during the test.

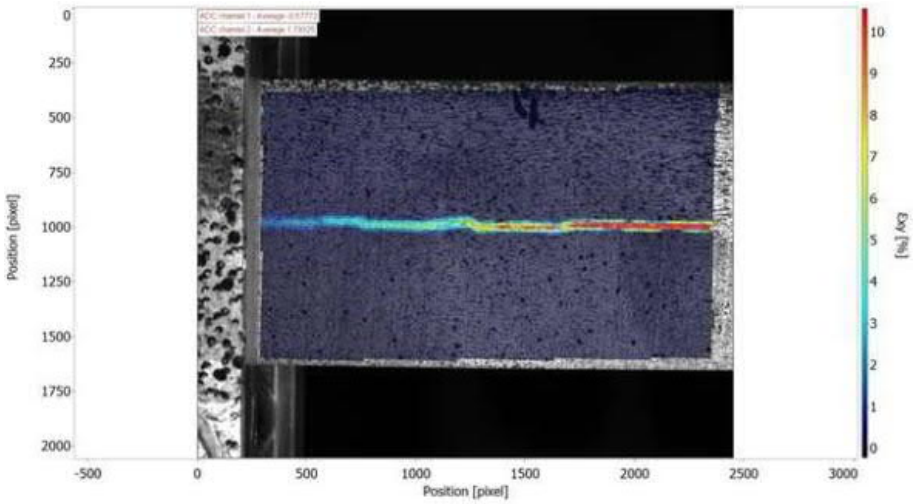

Figure 12 – Shear strain distribution at the last phase of test (*R*=-1, load 50 %).

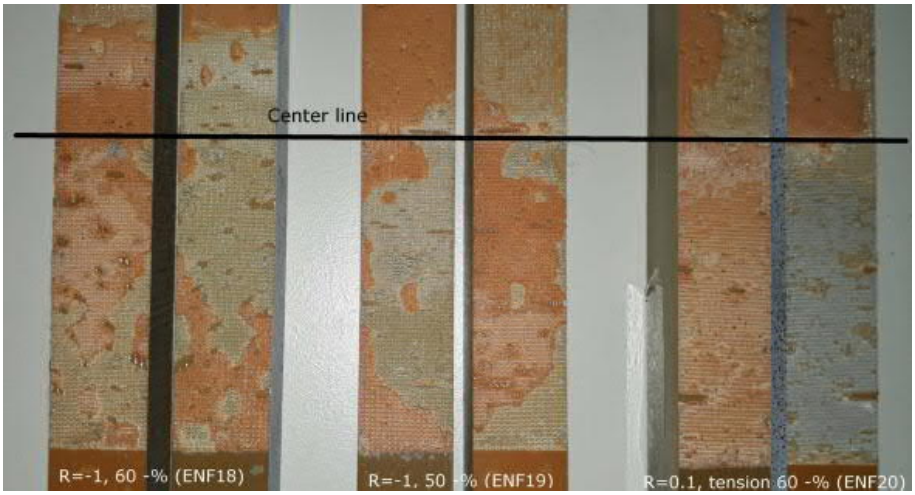

Figure 13 – Post-test fracture surfaces: *R*=-1 60 % (left), *R*=-1 50 % (middle) and *R*=0.1 60 % (right).

4. Discussion and conclusion

The test setup development that allows negative load ratio (*R*<0) to characterize fracture mode II fatigue testing was studied in this work. The new test setup was designed and compared based on the typical three-point bending. Both directions of test machine use was studied before focusing on the chance of loading direction (change of shear stress sign for the glue line in ENF specimen). Based on our results, the compliance of the test setup, in terms of deformations remains small under the maximum load level of 60 % of the quasi-static ultimate strength of the target ENF joint. The FE analysis was performed with the 60 % loading. Based on the FE analyses, deformation in the test jig seems to be insignificant. The specimen movement in experiments was not shown to be extensive under cyclic, fatigue loading.

The comparison of the developed test system and the traditional setup was shown to provide difference in the crack propagation related to fatigue loading (*R*=0.1). The traditional setup generated crack propagation similar to the 'average' behaviour between upwards and downwards test machine application with the new system. The crack propagation under *R*=-1 fatigue was shown to be significantly faster than that for *R*=0.1 tests at the same peak load level. The dramatic change highlights the importance of considering the negative load ratio.

For future research, the effects of the test setup will be studied in terms of different materials. The number of tested specimens was small for the conceptual validation in this work. For that reason, the number of test specimen series will be higher for making solid conclusions in terms of the particular (adhesive) material, failure modes and fatigue data scatter. This work considered only two load levels for providing crack propagation in a feasible test time. In future research, the decrease of load level should be considered. Especially, the definition of 'no-growth condition' level would be useful for aeroplane joint design purposes. Of course, it should be kept in mind that the *R*=-1 might be too harsh condition when considering aeroplane joints. The increase of testing time, of course, requires test resources but also crack length measurement should be continuous and precise.

Acknowledgements

The authors would like to acknowledge Finnish Defence Forces Logistics Command for the financial support.

5. Contact Author Email Address

Mailto: jarno.jokinen@tuni.fi

6. Copyright Statement

References

[1] B.R.K. Blackman, A.J. Kinloch, M. Paraschi, The determination of the mode II adhesive fracture resistance, GIIC, of structural adhesive joints: An effective crack length approach, Eng Fract Mech, 72 (2005), 877-897, https://doi.org/10.1016/j.engfracmech.2004.08.007

[2] H. Wang, T. Vu-Khanh, Use of end-loaded-split (ELS) test to study stable fracture behaviour of composites under mode II loading, Compos Struct, 36 (1996), 71-79, https://doi.org/10.1016/S0263-8223(96)00066-9

[3] P. Qiao, J. Wang, J. Davalos, Analysis of tapered ENF specimen and characterization of bonded interface fracture under Mode-II loading, Int J Solids Struct, 40 (2003), 1865-1884, https://doi.org/10.1016/S0020-7683(03)00031-3

[4] H.-B. Kim, K. Naito, H. Oguma, Mode II fracture toughness of two-part acrylic-based adhesive in an adhesively bonded joint: end-notched flexure tests under static loading, Fatigue Fract Eng M, 40 (2017), 1795-1808, https://doi.org/10.1111/ffe.12599

[5] B.D. Davidson, X. Sun, Effects of friction, geometry, and fixture compliance on the perceived toughness from three-and four-point bend end-notched flexure tests, J Reinf Plast Comp, 24 (2005), 1611-1628, https://doi.org/10.1177/0731684405050402

[6] M. Pérez-Galmés, J. Renart, C. Sarrado, A.J. Brunner, A. Rodríguez-Bellido, Towards a consensus on mode II adhesive fracture testing: Experimental study, Theor Appl Fract Mech, 98 (2018), 210–219, https://doi.org/10.1016/j.tafmec.2018.09.014

[7] O. Orell, J. Jokinen, M. Kanerva, Use of DIC in characterization of mode II crack propagation in adhesive fatigue testing, Int J Adhes Adhes, 2022, submitted for acceptance

[8] M. Dessureautt, K. Spelt, Observations of fatigue crack initiation and propagation in an epoxy adhesive, Int J Adhes Adhes, 17 (1997), 183-195, https://doi.org/10.1016/S0143-7496(96)00044-9

[9] I.Floros, K.Tserpes, Fatigue crack growth characterization in adhesive CFRP joints, Compos Struct, 207 (2019), 531-536, https://doi.org/10.1016/j.compstruct.2018.09.020

[10] M.C.Y. Niu, Stress Analysis of Airframe Structures. Hong Kong. Hong Kong Conmilit Press, 1997, ISBN 962-7128-08-2

[11] T. Nyman, H. Ansell, A. Blom, Effects of truncation and elimination on composite fatigue life. Compos Struct, 48 (2000), 275-286, https://doi.org/10.1016/S0263-8223(99)00115-4

[12] J. Jokinen, O. Orell, M. Wallin, M. Kanerva, A concept for defining mixed-mode behaviour of tough epoxy film adhesives by single specimen design, J Adhes Sci Technol, 34 (2020), 1982-1999, https://doi.org/10.1080/01694243.2020.1746606

[13] O. Ishai, H. Rosenthal, N. Sela, E. Drukker, Effect of selective adhesive inter-leaving on interlaminar fracture toughness of graphite/epoxy composite laminates, Composites 19 (1988), 49–54, https://doi.org/10.1016/0010-4361(88)90543-5